Optica Applicata, Vol. XXXI, No. 1, 2001

Optimization of detection system for low-coherence interferometric sensors based on highly birefringent fibers

MAGDALENA S. NAWROCKA, WACŁAW URBAŃCZYK

Institute of Physics, Wroclaw University of Technology, 50–370 Wrocław, Wybrzeże Wyspiańskiego 27, Poland.

A demodulation system employing birefringent crystalline plates for decoding low-coherence interferometric sensors based on highly birefringent fibers was numerically analyzed in order to find its optimum construction. A numerical approach proposed in this paper allowed us to calculate how the parameters of the decoding system such as thickness and orientation of the crystalline plates, type of birefringent material, position of the detectors, and polarization characteristics of beam splitting plates influence the contrast of differential interference signals. Calculations were based on vectorial ray tracing algorithm applicable to isotropic as well as anisotropic media. The algorithm allowed determination of intersection coordinates with detector surface for ordinary and extraordinary rays, their phases, polarizations, and amplitudes, and finally the contrast of differential interference signals. Based on modeling results, general principles concering system construction were formulated, which assure the highest possible contrast of interference signals and therefore maximum operation range of the sensor.

1. Introduction

Recently a flexible detection system was proposed [1] for decoding phase shifts induced in low-coherence interferometric sensors based on counting fractions (1/8 or 1/4) of interference fringes. The performance of the system was tested in measurements of hydrostatic pressure changes using a single temperature-compensated sensor [1] and also in simultaneous measurements of pressure and temperature changes using two serially multiplexed sensors [2]. The demodulation system proposed is composed of four detection channels containing crystalline quartz plates, which compensate for the optical path delay introduced by interrogated sensor. The problem of fading was solved by tilting the quartz plates, thereby introducing an initial phase shift between interference signals and finally allowing digital phase measurements with a resolution of 1/8 or 1/4 of an interference fringe, depending on the number of multiplexed sensors. The contrast of the differential interference signals registered in the detection channels is a crucial factor influencing the sensor operating range. For perfectly aligned sensor elements, the maximum contrast is equal to 0.5 [3], [4]. In real systems, however, the contrast of differential interference signals is much lower due to imperfect azimuth alignment of successive

sensor elements (typical alignment error equals 5°), convergence of the light beam in a detection system, and finally due to polarizations and amplitudes changes introduced by reflections from a beam-splitter and boundaries of the decoding plate. The complexity of the problem causes that analysis of contrast dependence upon all these factors can be performed in a numerical way only. For that purpose, we adopted the ray tracing method proposed in [5] for uniaxial birefringent media. From the results of our analysis we were able to establish several general principles concerning optimum construction of the decoding system.

2. Formulation of the problem

Construction of a system for decoding sensors based on highly birefringent fibers is illustrated in Fig. 1. To fulfil the coherence addressing principle [6] we use a broad-band superluminescent diode pigtailed with 3M polarizing fiber. Linearly

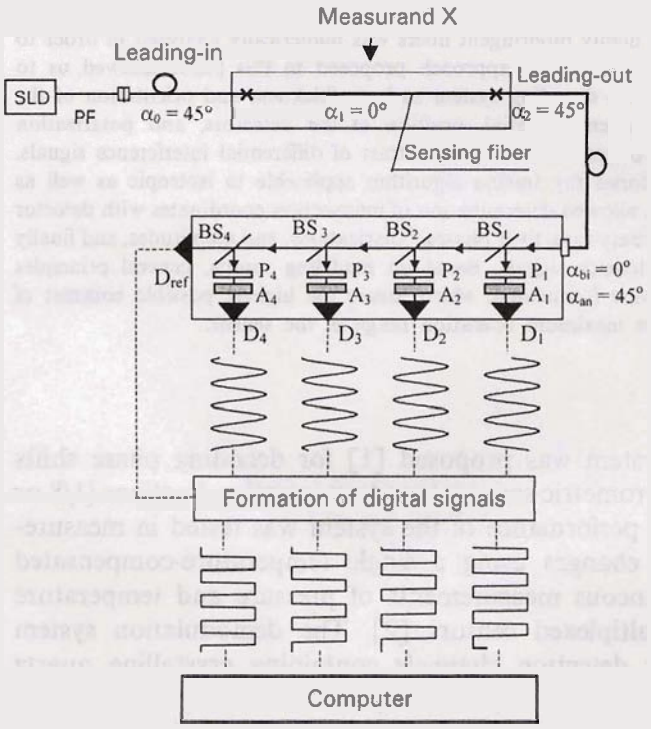

Fig. 1. Scheme of the system with four detection channels for decoding phase shifts induced in the sensing fiber by measurand changes: SLD – superluminescent diode, PF – polarizing fiber, BS_{1-4} – beam splitters, P_{1-4} – quartz delay plates, A_{1-4} – analyzers, D_{1-4}, D_{ref} – photodiodes.

polarized light from the polarizing fiber is coupled by a polarization maintaining connector into one mode of the leading-in fiber. This fiber and the active part of the sensor are spliced to each other with rotation of their polarization axes by

$\alpha_1 - \alpha_0 = -45°$. Therefore, two polarization modes are excited in the active element of the sensor, which in turn is spliced with a highly birefringent leading-out fiber with rotation of their polarization axes by $\alpha_2 - \alpha_1 = 45°$. The output of the leading-out fiber is aligned at $\alpha_{bi} - \alpha_2 = -45°$ with respect to the polarization axes of the quartz delay plates.

The detection system is composed of four channels for registering interference signals and one channel for measuring average intensity at the sensor output. In the system for decoding one sensor, all plates have the same thickness. The plates are tilted with respect to the incident beam in order to tune the initial phase shift of the interference signal in every decoding channel. The intensity variations observed in the detection channels may be expressed by the following equation:

$$I(\delta_S, \delta_R) = I_0[1 + V_{S/\pm R}\gamma(\Delta R_S \pm \Delta R_R)\cos(\delta_S \pm \delta_R) + V_S\gamma(\Delta R_S)\cos(\delta_S) + V_R\gamma(\Delta R_R)\cos(\delta_R)] \quad (1)$$

where I_0 is the average intensity, V_S, V_R indicate maximum contrast of interference signals associated with sensing and receiving interferometers, $V_{S/\pm R}$ is a maximum contrast of the differential and additive patterns, γ is a coherence function of the source, ΔR_S, ΔR_R and δ_S, δ_R are respectively optical path delays (OPD) and phase delays introduced by the sensing fiber and decoding plate. Equation (1) shows that the interference phenomenon can be observed in the detection channels only if the total optical path delay ΔR_S introduced by the sensor is compensated by the optical path delay ΔR_R introduced by the quartz plates. In such a case the intensity registered in the detection channels may be represented by the following equation:

$$I = \mathrm{I}_0[1 + V_{S/-R}\gamma(\Delta R_S - \Delta R_R)\mathrm{sins}(\delta_S - \delta_R)]. \quad (2)$$

The phase shifts δ_R introduced by the quartz plates in successive channels differ by $\pi/4$, which corresponds to 1/8 of an interference fringe. At the same time, the contrast of all interference signals remains practically the same because γ is a slowly changing function of OPD imbalance $(\Delta R_S - \Delta R_R)$ compared to the fast intensity variations associated with interference fringes. Sinusoidal intensity changes registered in the detection channels are converted into digital signals in such a way that a high level is generated when the interference signal is greater than the average intensity I_0 and the low level is generated for $I < I_0$. This version of the detection system allows measurement of the fast phase changes arising in a sensing fiber with a resolution of 1/8 of an interference fringe and easy recognition of the direction of phase changes.

The measuring range of the system is associated with the spectral characteristics of the source. Assuming a Gaussian shape of the source spectrum we can describe the degradation of the contrast with the increasing imbalance of OPD between the sensing and receiving interferometers in the following way [7]:

$$\gamma = \exp\left[-\left(\frac{\pi\delta\lambda}{2\sqrt{2\lambda_0}}\,\frac{\Delta R_S - \Delta R_R}{\lambda_0}\right)^2\right] \quad (3)$$

where $\Delta\lambda$ is the full spectral linewidth at half maximum of the Gaussian distribution and λ_0 is a central wavelength of the source. For proper operation of the electronic unit forming the digital pulses, the amplitude of the interference signal must be greater than 10% of average intensity. This requirement is equivalent to the following condition:

$$|\Delta R_S - \Delta R_R| < \frac{2\lambda_0^2\sqrt{2\ln(10V_{S/-R})}}{\pi\delta\lambda} \tag{4}$$

The OPD imbalance between x- and y-polarized modes introduced by the sensing fiber is given by

$$\Delta R_S = \Delta R_S^0 + \Delta R_S^X \tag{5}$$

where ΔR_S^0 is the initial OPD imbalance at zero value of the measurand applied and ΔR_S^X is an additional imbalance induced by the measurand X. Depending on the sign of ΔR_S^X the initial alignment of the system should satisfy one of the following conditions:

$$\Delta R_S^0 - \Delta R_R = \pm\frac{2\lambda_0^2\sqrt{2\ln V_{S/-R}}}{\pi\delta\lambda}, \tag{6}$$

for negative and positive ΔR_S^X, respectively. If the above condition is satisfied, the full range of the system is limited by the spectral linewidth of the source and by the maximum contrast of the differential pattern $V_{S/-R}$

$$\Delta R_{S_{\max}}^X = \frac{4\lambda_0^2\sqrt{2\ln 10V_{S/-R}}}{\pi\delta\lambda} \tag{7}$$

Maximum value of $V_{S/\pm R}$ equals 0.5 [3], [4] under condition that all the system elements are aligned as shown in Fig. 1 and there is no contrast degradation in the decoding system. For typical superluminescent diode we used $\lambda_0 = 832.5$ nm and $\delta\lambda = 17$ nm, which assures the theoretical operating range equal to 112 interference fringes ($\Delta R_{S_{\max}}^X = 112\lambda_0$). In practice, however, the operating range of our detection system was limited to about 52 fringes. This is associated with contrast degradation caused by the physical factors already mentioned in the introduction. According to Eq. (7) the contrast $V_{S/-R}$ is a crucial parameter influencing the operating range of sensors. Therefore it is important to find such a construction of the decoding system which assures the highest possible contrast $V_{S/-R}$ of the differential interference signal.

The light beam in the detection system has to be convergent (Fig. 2) in order to focus all energy on a photodetector active element, which is small to assure high frequency bandwidth. The convergent beam may be divided into a set of N rays (plane waves) incident on a decoding crystalline plate at different angles. Each of the rays will experience individual phase shift introduced by the decoding plate. In order to describe the contrast degradation caused by this effect, the output intensity is expressed as a sum of N interference signals

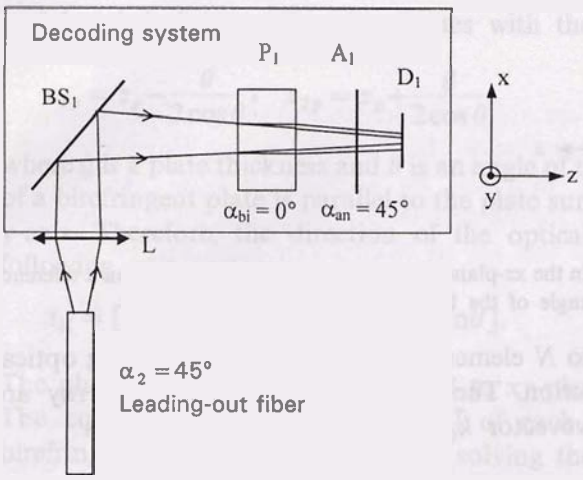

Fig. 2. Details of the first detection channel in the decoding system: α_{bi} — an angle between direction of the optical axis of the birefringent plate and y-axis of the coordinate system, α_{an} — an angle between transmission azimuth of the analyzer and y-axis of the coordinate system, L — imaging lens, BS_1 — beam splitting plate, P_1 — birefringent plate, A_1 — analyzer, D_1 — photodetector.

$$I(\delta_S,\delta_R)=\frac{1}{N}\sum_{i=1}^{N} I^i[1+V^i_{S/\pm R}\gamma(\Delta R_S\pm\Delta R^i_R)\cos(\delta_S\pm\delta^i_R) + V^i_S\gamma(\Delta R_S)\cos(\delta_S)+V^i_R\gamma(\Delta R^i_R)\cos(\delta^i_R)]. \tag{8}$$

Calculations of phase shifts δ^i_R introduced by crystalline plate (quartz or calcite) were carried out using vectorial algorithm first proposed in [5]. We also took into account polarization changes introduced by the beam splitter and boundaries of the decoding plate. To shorten the time of calculations we assumed the light source to be strictly monochromatic. In such a case, the coherence functions in Eq. (8) are equal to 1 and the output intensity may be expressed as

$$I(\delta_S,\delta_R)=\frac{1}{N}\sum_{i=1}^{N} I^i[1+V^i_{S/\pm R}\cos(\delta_S\pm\delta^i_R)+V^i_S\cos(\delta_S)+V^i_R\cos(\delta^i_R)]. \tag{9}$$

To extract from the above expression the intensity variation associated with the differential interference signal we used a specially developed procedure employing numerical modulation of the phase shifts δ_S and δ^i_R and Fourier analysis.

3. Ray tracing algorithm

We assumed that the lens transforming the divergent light beam coming out from the output of the fiber sensor into convergent beam incident on the detector is aberration free and that this convergent beam is focused in the origin of x-y-z coordinate system, Fig. 3. The aperture angle of the convergent beam is equal to β. Such a beam can be represented as a sphere with the center at point (0, 0 ,0) and the

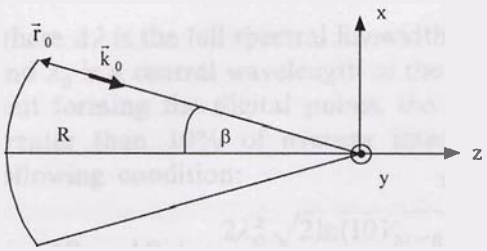

Fig. 3. Cross-section of the reference sphere in the xz-plane; $\vec{r}_0$ — initial position of the ray on a reference sphere, $\vec{k}_0$ — wavevector, β — aperture angle of the beam in a detection system.

radius R. This sphere is divided into N elements, each of them representing optical ray (plane wave) of different direction. The initial coordinates of each ray are represented by $\vec{r}_0$ and by the wavevector $\vec{k}_0$, which can be expressed as

$$\vec{k}_0 = \frac{2\pi}{\lambda_0}\frac{\vec{r}_0}{|\vec{r}_0|} \tag{10}$$

where $\lambda_0 = 832.5$ nm is central wavelength of a broad-band light source. The aim of the ray tracing analysis is to find for each ray its intersection coordinates with the first and the second surface of the decoding plate and finally with the photodetector plane, Fig. 4. We assume that the rotation axis of the birefringent plate is located

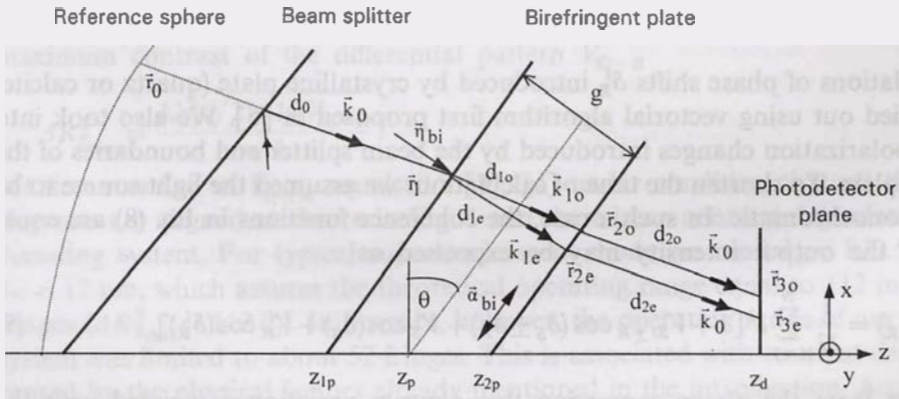

Fig. 4. Path of the optical ray from the reference sphere to the photodetector, $\vec{r}$ — coordinates of ray intersection with successive surfaces, $\vec{k}$ — wavevectors, d — geometrical distances between successive surfaces, $\vec{\eta}_{bi}$ — unit vector normal to the birefringent plate, θ — rotation angle of the birefringent plate, g — thickness of the plate, $\vec{a}_{bi}$ — unit vector representing optical axis, z_p — position of rotation axis of the birefringent plate, z_{1p}, z_{2p}, z_d — coordinates of the first and the second surfaces of the birefringent plate and the photodetector.

in half of its thickness, overlaps with y-axis of a coordinate system, and intersects the z-axis at point z_p. In such a case, the two surfaces of the birefringent plate may be represented by the normal vector

$$\vec{\eta}_{bi} = [-\sin\theta \quad 0 \quad \cos\theta] \tag{11}$$

and by their intersection coordinates with the z-axis:

$$z_{1p} = z_p - \frac{g}{2\cos\theta}, \quad z_{2p} = z_p + \frac{g}{2\cos\theta} \tag{12}$$

where g is a plate thickness and θ is an angle of the plate with x-axis. The optical axis of a birefringent plate is parallel to the plate surface and makes an angle α_y with the y-axis. Therefore, the direction of the optical axis may be represented by the following unit vector:

$$\vec{\alpha}_{bi} = [\sin\alpha_y \cos\theta \quad \cos\alpha_y \quad \sin\alpha_y \sin\theta]. \tag{13}$$

The photodetector surface is parallel to xy-plane and intersects z-axis at point z_d. The coordinates of intersection ($\vec{r}_1$) of each ray with the first surface of the birefringent plate may be found by solving the following set of linear equations:

$$\begin{cases} (\vec{r}_1 - z_{1p}\vec{z})\,\vec{\eta}_{bi} = 0 \\ \vec{r} = \vec{r}_0 + d_0 \dfrac{\vec{k}_0}{|\vec{k}_0|} \end{cases} \tag{14}$$

where $\vec{z}$ is a versor of z-axis, and d_0 is a geometrical way of the ray from reference sphere to intersection point. Analytical solutions for $\vec{r}_1$ and d_0 are as follows:

$$\vec{r}_1 = \vec{r}_0 + d_0 \frac{\vec{k}_0}{|\vec{k}_0|}, \quad d_0 = \frac{z_{1p}\vec{z}\vec{\eta}_{bi} - \vec{r}_0\vec{\eta}_{bi}}{\dfrac{\vec{k}_0}{|\vec{k}_0|}\vec{\eta}_{bi}} \tag{15}$$

In the next step of calculations, wavevectors $\vec{k}_{1o}$ and $\vec{k}_{1e}$ for the corresponding ordinary and extraordinary waves in the birefringent plate are determined. To find these two vectors we used the formalism first proposed in [5], according to which $\vec{k}_{1o}$ and $\vec{k}_{1e}$ may be expressed by the following relations:

$$\vec{k}_{1o} = \vec{k}_0 + \frac{2\pi}{\lambda_0}\Gamma_{1o}\vec{\eta}_{bi}, \tag{16}$$

$$\vec{k}_{1e} = \vec{k}_0 + \frac{2\pi}{\lambda_0}\Gamma_{1e}\vec{\eta}_{bi} \tag{17}$$

where Γ_{1o}, Γ_{1e} are positive roots of the following equations:

$$\Gamma_{1e}^2[1 + q(\vec{\eta}_{bi}\vec{\alpha}_{bi})^2] + 2\Gamma_{1e}[\vec{N}_0\vec{\eta}_{bi} + q(\vec{N}_0\vec{\alpha}_{bi})(\vec{\eta}_{bi}\vec{\alpha}_{bi}) + |\vec{N}_0|^2 - n_e^2 + q(\vec{N}_0\vec{\alpha}_{bi})^2 = 0 \tag{18}$$

and

$$\Gamma_{1o}^2 + 2\Gamma_{1o}(\vec{N}_0\vec{\eta}_{bi}) + |\vec{N}_0|^2 - n_{1o}^2 = 0 \tag{19}$$

where the parameter q is given by

$$q = \frac{n_{1e}^2 - n_{1o}^2}{n_{1o}^2}. \tag{20}$$

In the above equations, n_{1o} and n_{1e} are ordinary and extraordinary refractive indices of the birefringent plate. For ordinary wave, the direction of the Poynting vector (direction of optical ray) overlaps with $\vec{k}_{1o}$. By analogy to Eqs. (14), (15) the intersection coordinates $\vec{r}_{2o}$ with the second surface of birefringent plate for ordinary ray and the geometrical way d_{1o} of this ray in birefringent plate can be found in a straightforward way:

$$\vec{r}_{2o} = \vec{r}_1 + d_{1o}\frac{\vec{k}_{1o}}{|\vec{k}_{1o}|}, \quad d_{1o} = \frac{z_{2p}\vec{z}\vec{\eta}_{bi} - \vec{r}_1\vec{\eta}_{bi}}{\frac{\vec{k}_{1o}}{|\vec{k}_{1o}|}\vec{\eta}_{bi}} \tag{21}$$

The direction of extraordinary ray $\vec{\rho}_{1e}$ does not overlap with $\vec{k}_{1e}$. However, using formalism proposed in [5], $\vec{\rho}_{1e}$ can be found from the following equation:

$$\vec{\rho}_{1e} = n_{1e}^2\left(\frac{\vec{k}_{1e}\vec{\alpha}_{bi}}{|\vec{k}_{1e}|}\right)\vec{\alpha}_{bi} + n_{1o}^2\left[\frac{\vec{k}_{1e} - (\vec{k}_{1e}\vec{\alpha}_{bi})\vec{\alpha}_{bi}}{|\vec{k}_{1e}|}\right]. \tag{22}$$

If $\vec{\rho}_{1e}$ is known, the intersection coordinates $\vec{r}_{2e}$ of the extraordinary ray with the second surface of birefringent plate, the geometrical way d_{1e} of this ray in birefringent plate and its refractive index n_ρ can be determined from the following equations:

$$\vec{r}_{2e} = \vec{r}_1 + d_{1e}\frac{\vec{\rho}_{1e}}{|\vec{\rho}_{1e}|}, \quad d_{1e} = \frac{z_{2p}\vec{z}\vec{\eta}_{bi} - \vec{r}_1\vec{\eta}_{bi}}{\frac{\vec{\rho}_{1e}}{|\vec{\rho}_{1e}|}\vec{\eta}_{bi}}, \quad n_\rho = \frac{\lambda_0}{2\pi|\vec{\rho}_{1e}|}\vec{N}_{1e}\vec{\rho}_{1e}. \tag{23}$$

Having passed the birefringent plate, the ordinary and extraordinary rays propagate again in the direction $\vec{k}_0$. Their intersection coordinates with the detector surface are given by:

$$\vec{r}_{3o} = \vec{r}_{2o} + d_{2o}\frac{\vec{k}_0}{|\vec{k}_0|}, \quad d_{2o} = \frac{z_d\vec{z}\vec{\eta}_d - \vec{r}_{2o}\vec{\eta}_d}{\frac{\vec{k}_0}{|\vec{k}_0|}\eta_d}, \tag{24}$$

$$\vec{r}_{3e} = \vec{r}_{2e} + d_{2e}\frac{\vec{k}_0}{|\vec{k}_0|}, \quad d_{2e} = \frac{z_d\vec{z}\vec{\eta}_d - \vec{r}_{2e}\vec{\eta}_d}{\frac{\vec{k}_0}{|\vec{k}_0|}\vec{\eta}_d} \tag{25}$$

where $\vec{\eta}_d = [0\ 0\ 1]$ is a unit vector perpendicular to the detector surface.

If the geometrical ways for ordinary and extraordinary rays are known we can easily calculate the respective phase shifts:

$$\Delta\Phi_o = \frac{2\pi}{\lambda_0}(d_0 + d_{1o}n_o + d_{2o}), \tag{26}$$

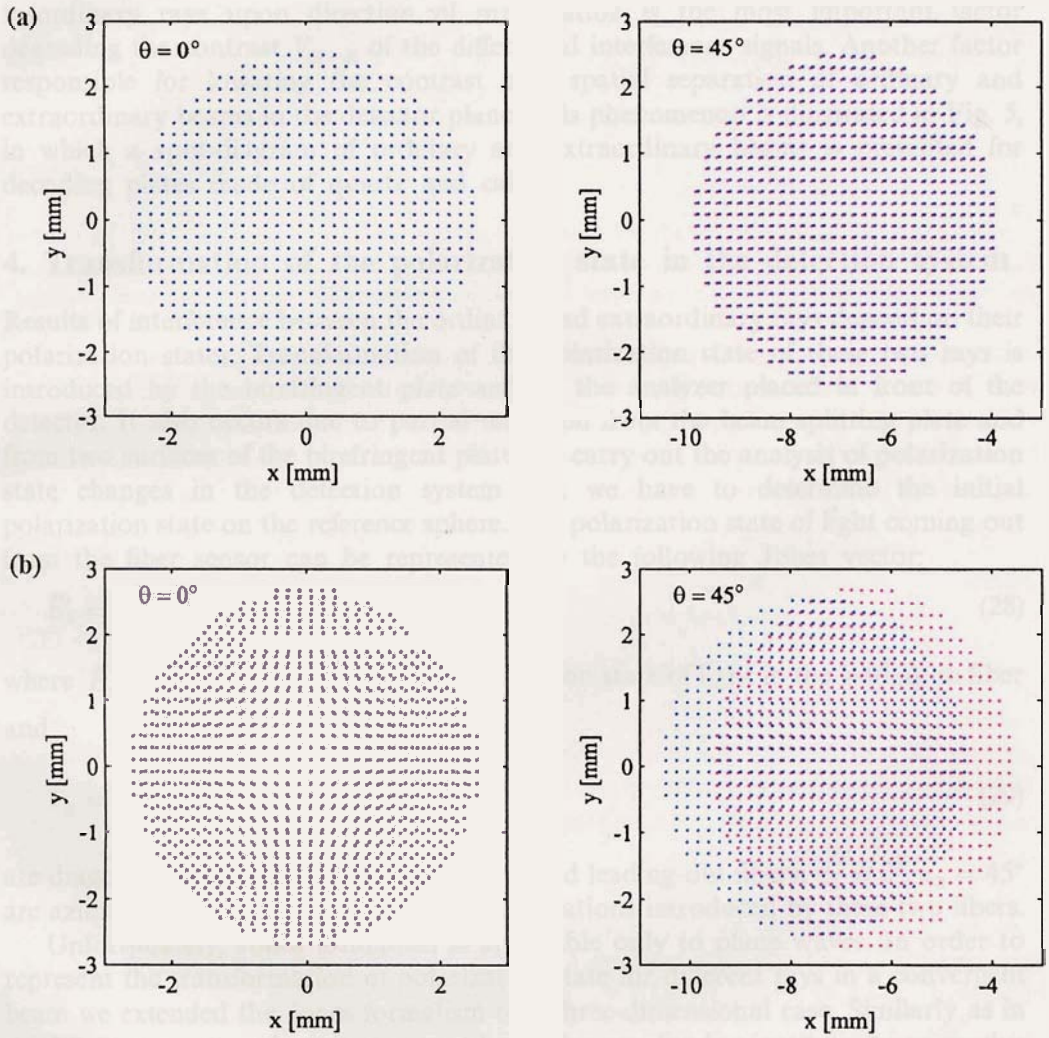

Fig. 5. Spot-diagram for ordinary (blue) and extraordinary (red) rays in the photodetector plane. The calculations were carried out for quartz (**a**) and calcite (**b**) delay plate for rotation angles $\theta = 0°$ and $\theta = 45°$. The other parameters of the detecting system were as follows: aperture angle $\beta = 5°$, plate thickness $g = 20$ mm, orientation of optical axis $\alpha_{hi} = 0°$.

$$\Delta\Phi_e = \frac{2\pi}{\lambda_0}(d_0 + d_{1e}n_\rho + d_{2e}). \tag{27}$$

The dependence of the phase shifts between interfering ordinary and extraordinary rays upon direction of propagation is the most important factor degrading the contrast $V_{S/-R}$ of the differential interference signals. Another factor responsible for lowering the contrast is a spatial separation of ordinary and extraordinary beams in the detector plane. This phenomenon is illustrated in Fig. 5, in which a spot-diagram of ordinary and extraordinary beams is presented for decoding plates made of quartz and calcite.

4. Transformation of the polarization state in the detection system

Results of interference between the ordinary and extraordinary rays depend on their polarization states. Transformation of the polarization state of these two rays is introduced by the birefringent plate and by the analyzer placed in front of the detector. It also occurs due to partial reflection from the beam splitting plate and from two surfaces of the birefringent plate. To carry out the analysis of polarization state changes in the detection system first we have to determine the initial polarization state on the reference sphere. The polarization state of light coming out from the fiber sensor can be represented by the following Jones vector:

$$\vec{E}'_S = \mathbf{R}(\alpha_2)\mathbf{T}_{\text{out}}\mathbf{R}(-\alpha_2)\mathbf{R}(\alpha_1)\mathbf{T}_S\mathbf{R}(-\alpha_1)\vec{E}_p, \tag{28}$$

where $\vec{E}_p = \begin{bmatrix} \cos\alpha_0 \\ \sin\alpha_0 \end{bmatrix}$ represents the polarization state of light in the leading-in fiber and

$$\mathbf{T}_S = \begin{bmatrix} e^{i\delta_S} & 0 \\ 0 & 1 \end{bmatrix}, \quad \mathbf{T}_{\text{out}} = \begin{bmatrix} e^{i\delta_{\text{out}}} & 0 \\ 0 & 1 \end{bmatrix} \tag{29}$$

are diagonal Jones matrices for the sensing and leading-out fibers, $\alpha_1 = 0°$, $\alpha_2 = 45°$ are azimuths and δ_S, δ_{out} are the phase retardations introduced by these two fibers.

Unfortunately, Jones formalism is applicable only to plane waves. In order to represent the transformation of polarization state for different rays in a convergent beam we extended the Jones formalism to a three-dimensional case. Similarly as in the 2D case, x-, y-, and z-components of complex amplitude constitute the respective elements of the 3D vector. For collimated rays coming out from the output of the fiber-optic sensor, the components of the three-dimensional Jones vector are associated with the components of the two-dimensional vector $\vec{E}'_S$ in the following way:

$$\vec{E}_S = \begin{bmatrix} (E'_S)_x \\ (E'_S)_y \\ 0 \end{bmatrix}. \tag{30}$$

To find the relation between three-dimensional vector $\vec{E}_S$ created in this way and the

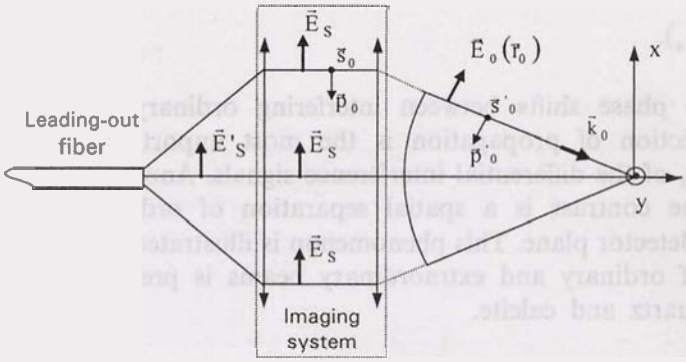

Fig. 6. Transformation of two-dimensional vector $\vec{E}_S'$ representing polarization state at the output of the leading-out fiber into three-dimensional vector $\vec{E}_0$ representing polarization state on the reference sphere.

vector $\vec{E}_0$ representing the polarization state on the reference sphere we divide $\vec{E}_S$ into $\vec{p}$ and $\vec{s}$ components, Fig. 6. One should note that transformation of the collimated beam into convergent one involves change of direction only for components of the complex amplitude. Therefore, the relation between $\vec{E}_S$ and $\vec{E}_0$ is given by the following equation:

$$\vec{E}_0 = (\vec{E}_S \vec{s}_0)\vec{s}_0' + (\vec{E}_S \vec{p}_0)\vec{p}_0' \tag{31}$$

where:

$$\vec{s}_0 = \frac{\vec{k}_0 \times \vec{z}}{|\vec{k}_0 \times \vec{z}|}, \quad \vec{p}_0 = \frac{\vec{z} \times \vec{s}_0}{|\vec{z} \times \vec{s}_0|}, \tag{32}$$

$$\vec{s}_0' = \vec{s}_0, \qquad \vec{p}_0' = \frac{\vec{k}_0 \times \vec{s}_0'}{|\vec{k}_0 \times \vec{s}_0'|}. \tag{33}$$

The beam splitting plate is aligned at the angle $\alpha_{bs} = 45°$ with respect to z-axis of the coordinate. Its surface may be represented by the normal vector

$$\vec{\eta}_{bs} = [-\sin\alpha_{bs} \quad 0 \quad \cos\alpha_{bs}]. \tag{34}$$

For every ray reflected by the splitting plate, the incidence plane is determined by two vectors $\vec{p}_{bs}$ and $\vec{k}_0$, while vectors $\vec{s}_{bs}$ and $\vec{k}_0$ lie in the plane perpendicular to the incidence plane. Vectors $\vec{s}_{bs}$ and $\vec{p}_{bs}$ are given by:

$$\vec{s}_{bs} = \frac{\vec{k}_0 \times \vec{\eta}_{bs}}{|\vec{k}_0 \times \vec{\eta}_{bs}|}, \quad \vec{p}_{bs} = \frac{\vec{k}_0 \times \vec{s}_{bs}}{|\vec{k}_0 \times \vec{s}_{bs}|}. \tag{35}$$

To avoid unnecessary complications in ray tracing algorithm, we assumed that the beam splitting plate operates in a transmission mode, however, the polarization changes it introduces are the same as in the reflection mode and may by represented by the following expression:

$$\vec{E}_{bs} = \frac{|r_p|}{|r_s|} e^{i\Delta} (\vec{E}_0 \vec{p}_{bs})\vec{p}_{bs} + (\vec{E}_0 \vec{s}_{bs})\vec{s}_{bs} \tag{36}$$

where r_p, r_s are reflection coefficients, and Δ is a phase shift occurring between $\vec{p}$ and $\vec{s}$ and components of reflected amplitude. The parameters $|r_p|/|r_s|$ and Δ were determined experimentally as a function of incidence angle using the ellipsometric method. The measurements were carried out for a typical beam splitting plate that was used in detection system, Fig. 7. Taking into account polarization changes introduced by the beam splitting plate, the complex amplitude on first surface of birefringent plate may be expressed as

$$\vec{E}_{r1} = \vec{E}_{bs} \exp\left(\pm i \frac{2\pi}{\lambda_0} d_0 \right) \tag{37}$$

where d_0 is a distance from the reference sphere to the first surface of birefringent plate.

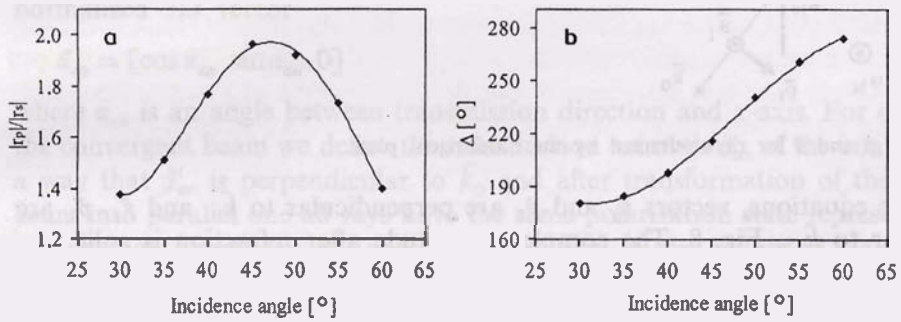

Fig. 7. Results of measurement of $|r_p|/|r_s|$ and Δ versus incidence angle for the beam splitting plate used in the decoding system.

The polarization changes occurring on this surface are associated with partial reflection and division of amplitude into ordinary and extraordinary waves. To describe polarization changes due to partial reflection we disregarded birefringence of the plate and used the well known Fresnel transmission coefficients [8]:

$$t_{1s} = \sqrt{\frac{\vec{k}_{1o}\vec{\eta}_{bi}}{\vec{k}_0\vec{\eta}_{bi}}} \frac{2\vec{k}_0\vec{\eta}_{bi}}{\vec{k}_0\vec{\eta}_{bi} + \vec{k}_{1o}\vec{\eta}_{bi}}, \tag{38}$$

$$t_{1p} = \sqrt{\frac{\vec{k}_{1o}\vec{\eta}_{bi}}{\vec{k}_0\vec{\eta}_{bi}}} \frac{2\vec{k}_0\vec{\eta}_{bi}}{n_0\left(\frac{\vec{k}_{1o}}{n_{1o}}\vec{\eta}_{bi}\right) + n_{1o}\left(\frac{\vec{k}_0}{n_0}\vec{\eta}_{bi}\right)}. \tag{39}$$

In the above equations, $\vec{\eta}_{bi}$ is a vector normal to the birefringent plate, n_0 is a refractive index in the air, n_{1o} and $\vec{k}_{1o}$ are respectively the refractive index the and the wave vector for refracted ordinary wave. After passing the boundary of birefringent plate, the complex amplitude may be expressed as follows:

$$\vec{E}_1 = t_{1p}(\vec{E}_{r1}\vec{p}_1)\vec{p}'_1 + t_{1s}(\vec{E}_{r1}\vec{s}_1)\vec{s}'_1 \tag{40}$$

where:

$$\vec{s}_1' = \frac{\vec{\eta}_{bi} \times \vec{k}_{1o}}{|\vec{\eta}_{bi} \times \vec{k}_{1o}|}, \quad \vec{p}_1' = \frac{\vec{s}_1' \times \vec{k}_{1o}}{|\vec{s}_1' \times \vec{k}_{1o}|},$$
$$\vec{s}_1 = \frac{\vec{\eta}_{bi} \times \vec{k}_0}{|\vec{\eta}_{bi} \times \vec{k}_0|}, \quad \vec{p}_1 = \frac{\vec{s}_1 \times \vec{k}_0}{|\vec{s}_1 \times \vec{k}_0|}. \tag{41}$$

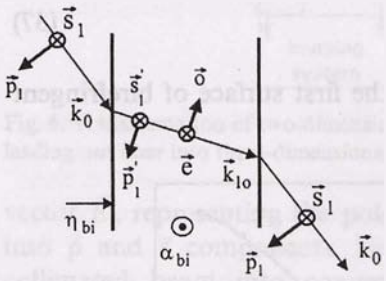

Fig. 8. Vectors $\vec{p}$ and $\vec{s}$ for rays refracted by the birefringent plate.

In the above equations, vectors $\vec{s}_1$ and $\vec{p}_1$ are perpendicular to $\vec{k}_0$, and $\vec{s}_1'$, $\vec{p}_1'$ are perpendicular to $\vec{k}_{1o}$, Fig. 8. The complex amplitude after refraction is split into ordinary and extraordinary components according to the following equation [8]:

$$\vec{E}_{1o} = (\vec{E}_1 \vec{o})\vec{o}, \quad \vec{E}_{1e} = (\vec{E}\vec{e})\vec{e} \tag{42}$$

where $\vec{o}$ and $\vec{e}$ and are the unit vectors representing polarization direction for ordinary and extraordinary waves:

$$\vec{o} = \frac{\vec{\alpha}_{bi} \times \vec{k}_{1o}}{|\vec{\alpha}_{bi} \times \vec{k}_{1o}|}, \quad \vec{e} = \frac{\vec{o} \times \vec{k}_{1o}}{|\vec{o} \times \vec{k}_{1o}|}. \tag{43}$$

In deriving Equation (43) we assume that birefringence of the decoding plate is not high and therefore the directions of $\vec{k}_{1o}$ and $\vec{k}_{1e}$ are almost the same.

If $\vec{E}_{1o}$ and $\vec{E}_{1e}$ are known, the complex amplitudes on the second surface of the birefringent plate are given by:

$$\vec{E}_{r2o} = \vec{E}_{1o} \exp\left(-i\frac{2\pi}{\lambda_0} n_{1o} d_{1o}\right), \quad \vec{E}_{r2e} = \vec{E}_{1e} \exp\left(-i\frac{2\pi}{\lambda_0} n_\rho d_{1e}\right) \tag{44}$$

where d_{1o}, d_{1e} and n_{1o}, n_ρ are respectively the geometrical ways and refractive indices of the ordinary and extraordinary rays in the birefringent plate. Knowing the transmission coefficients t_{2s} and t_{2p} on the second surface of the birefringent plate, which are represented by:

$$t_{2s} = \sqrt{\frac{\vec{k}_0 \vec{\eta}_{bi}}{\vec{k}_{1o} \vec{\eta}_{bi}}} \frac{2\vec{k}_{1o} \vec{\eta}_{bi}}{\vec{k}_{1o} \vec{\eta}_{bi} + \vec{k}_0 \vec{\eta}_{bi}}, \tag{45}$$

$$t_{2p} = \sqrt{\frac{\vec{k}_0 \vec{\eta}_{bi}}{\vec{k}_{1o} \vec{\eta}_{bi}}} \frac{2\vec{k}_{1o} \vec{\eta}_{bi}}{n_{1o}\left(\frac{\vec{k}_0}{n_0} \vec{\eta}_{bi}\right) + n_0\left(\frac{\vec{k}_{1o}}{n_{1o}} \vec{\eta}_{bi}\right)}, \tag{46}$$

we can finally determine the complex amplitude for ordinary and extraordinary waves at the output of the plate:

$$\vec{E}_{2o} = t_{2p}(\vec{E}_{r2o} \vec{p}'_1)\vec{p}_1 + t_{2s}(\vec{E}_{r2o} \vec{s}'_1)\vec{s}_1, \tag{47}$$

$$\vec{E}_{2e} = t_{2p}(\vec{E}_{r2e} \vec{p}'_1)\vec{p}_1 + t_{2s}(\vec{E}_{r2e} \vec{s}'_1)\vec{s}_1. \tag{48}$$

An analyzer placed in front of the photodetector is the last element changing polarization state of light in the detection system. For the ray passing along z-axis of the coordinate system the transmission azimuth of the analyzer is represented by the normalized 3D vector

$$\vec{\alpha}_{an} = [\cos\alpha_{an} \ \sin\alpha_{an} \ 0] \tag{49}$$

where α_{an} is an angle between transmission direction and x-axis. For other rays in the convergent beam we define the transmission azimuth $\vec{\alpha}'_{an}$ of the analyzer in such a way that $\vec{\alpha}'_{an}$ is perpendicular to $\vec{k}_0$ and after transformation of the convergent beam into parallel one all rays have the same polarization state represented by $\vec{\alpha}_{an}$. Under such conditions $\vec{\alpha}_{an}$ and $\vec{\alpha}'_{an}$ are related in the following way:

$$\vec{\alpha}'_{an} = (\vec{\alpha}_{an} \vec{s}_0)\vec{s}'_0 + (\vec{\alpha}_{an} \vec{p}_0)\vec{p}'_0. \tag{50}$$

The amplitudes of ordinary and extraordinary rays in the photodetector plane may be represented by:

$$\vec{E}_{r3o} = \vec{E}_{2o} \exp\left(-i\frac{2\pi}{\lambda_0} n_0 d_{2o}\right), \quad \vec{E}_{r3e} = \vec{E}_{2e} \exp\left(-i\frac{2\pi}{\lambda_0} n_0 d_{2e}\right) \tag{51}$$

where d_{2o}, d_{2e} are the respective geometrical distances calculated according to Eqs. (24), (25). After passing the analyzer these two amplitudes may be expressed as the following scalar products:

$$E_{3o} = \vec{\alpha}'_{an} \vec{E}_{3ro}, \quad E_{3e} = \vec{\alpha}'_{an} \vec{E}_{3re}, \tag{52}$$

and the total intensity registered by the photodetector is a sum of N waves (rays), for which the reference sphere was divided

$$I = \sum_{i=1}^{N} |E^i_{3o}|^2 + \sum_{i=1}^{N} |E^i_{3e}|^2 + 2\mathrm{Re} \sum_{i=1}^{N} E^i_{3e} E^{i*}_{3o}. \tag{53}$$

In the above expression, the first two summations are carried out over the total surface of the ordinary and extraordinary beams, while the third summation, representing the interference signals is carried out only over the common part of these two beams. Total intensity calculated according to Eq. (53) contains infor-

mation about all interference signals. The method of extracting the differential interference signal and calculating its contrast $V_{S/-R}$ and initial phase shift $\delta_S-\delta_R$ is described in the next subsection.

5. Determining the contrast of the differential interference pattern using Fourier analysis

To shorten the processing time we calculated the output intensity according to Eq. (53) only for one wavelength, *i.e.*, the central wavelength λ_0 of the light source. In such a case the coherence functions in Eq. (8) are equal to 1 and the output intensity is a superposition of several interference signals. To eliminate the interference signals associated with leading-out fibers we calculate the output intensity twice, first assuming that the light propagates in LP^x_{01} mode of the leading -out fiber and second, assuming that it propagates in LP^y_{01} mode. Finally, the two intensities are added to each other. Such a procedure assures that the output intensity contains only four interference signals, as expressed in Eq. (9). To extract the differential interference signal we used a numerical modulation of the phase shifts δ_S and δ^i_R and the Fourier analysis. The output intensity represented by Eq. (9) was calculated M times for different values δ_S and δ^i_R that are given by:

$$\delta^k_S = \delta_S+\varphi^k, \quad k=1, \ldots, M, \tag{54}$$

$$\delta^{ik}_R = \delta_R+3\varphi^k, \quad k=1, \ldots, M \tag{55}$$

where φ^k is a phase increment:

$$\varphi^k = \frac{2\pi}{M}k, \quad k=1, \ldots, M. \tag{56}$$

If δ_S and δ^i_R are numerically modulated, the output intensity contains four harmonics components: $I^k_S(\delta_S+\varphi^k)$, $I^k_{S/-R}(\delta_S-\delta_R-2\varphi^k)$, $I^k_R(\delta_R+3\varphi^k)$, $I^k_{S/+R}(\delta_S+\delta_R+4\varphi^k)$, which correspond to interference signals associated with the sensing interferometer, receiving interferometer, their difference (differential signal) and sum, respectively. On the other hand, the output intensity may be expressed as

$$I^k = I_0[1+V_S\cos(\delta_S+\varphi^k)+V_{S/-R}\cos(\delta_S-\delta_R-2\varphi^k) + V_R\cos(\delta_R+3\varphi^k)+V_{S/+R}\cos(\delta_S+\delta_R+4\varphi^k)]. \tag{57}$$

Applying Fourier analysis at elementary level we can easily extract the information about initial phase shift $\delta_S-\delta_R$ and the contrast $V_{S/-R}$ of the differential interference signal:

$$\delta_S-\delta_R = \arctan\frac{\sum_{k=0}^{M-1} I^k\sin\left(\frac{4k\pi}{M}\right)}{\sum_{k=0}^{M-1} I^k\cos\left(\frac{4k\pi}{M}\right)} \tag{58}$$

and

$$V_{S/-R} = \frac{\sum_{k=0}^{M-1} I^k \cos\left(\frac{4k\pi}{M}\right)}{I_0 \cos(\delta_S - \delta_R)} . \tag{59}$$

This procedure was used in modeling the contrast behaviour depending on different parameters of the detection system.

6. Results of modeling

In the first step of the detection system modeling optimum azimuths of all system elements with respect to the beam splitting plate were found. Based on the results of analytical considerations [3], [4], it was assumed that the successive elements of the fiber sensor and the detection system are aligned with rotation of polarization axes by 45°. The parameter α was introduced to represent rotation of all sensor elements with respect to the beam splitting plate:

$$\alpha_0 = \alpha - 45°,\ \alpha_1 = \alpha - 90°,\ \alpha_2 = \alpha - 45°,\ \alpha_y = \alpha - 90°,\ \alpha_{an} = \alpha - 45°. \tag{60}$$

The behaviour of the contrast $V_{S/-R}$ versus parameter α is presented in Fig. 9. Maximum values of $V_{S/-R}$ are equal to 0.5 and 0.41 respectively, for $\alpha = 45°$ and $\alpha = 0°$ or 90°. In the first case, $\vec{s}$, $\vec{p}$, directions for the central ray incident on the beam splitting plate overlap with the polarization directions of the eigenmodes in the leading-out fiber. In the second case, they overlap with polarization directions of the ordinary and extraordinary waves in the birefringent plate. In real detection system, for constructional reasons we applied the second configuration ($\alpha = 90°$) assuring a slightly lower contrast. Further analysis of the detection system is carried out under assumption that $\alpha = 90°$.

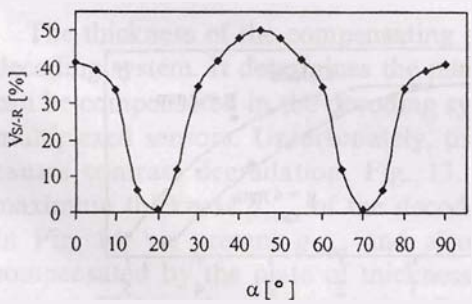

Fig. 9. Contrast $V_{S/-R}$ of the differential interference pattern versus parameter α representing rotation of all system elements with respect to the beam-splitting plate. The calculations were carried out for the following parameters of the system: aperture angle $\beta = 2.5°$, thickness of the decoding quartz plate $g = 4$ mm, rotation angle of the plate $\theta = 0°$.

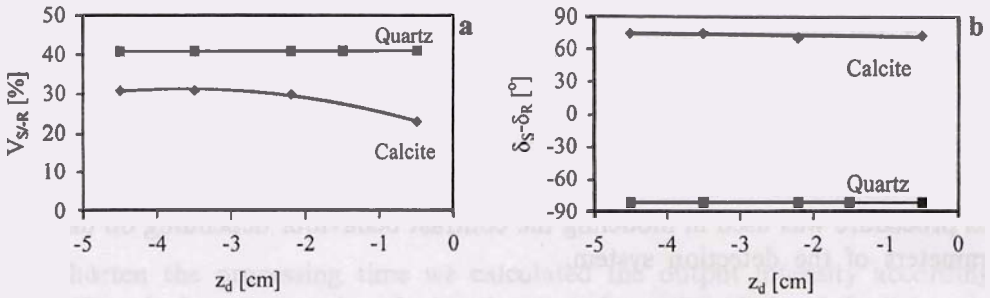

Fig. 10. Contrast $V_{S/-R}$ (a) and initial phase shift $\delta_S - \delta_R$ (b) of the differential interference pattern versus position of the detector z_d. The calculations were carried out for the following parameters of the system: aperture angle $\beta = 2.5°$, thickness of the decoding plates $g = 4$ mm, rotation angle of the plates $\theta = 0$.

In the second step of modeling, the contrast $V_{S/-R}$ was optimized with respect to position of the detector z_d. The calculations of $V_{S/-R}$ and $\delta_S - \delta_R$ were carried out for different parameters of the detection system. As an example we show in Fig. 10 the calculation results for calcite and quartz decoding plates of thickness $g = 4$ mm, aperture angle $\beta = 2.5°$ and the following azimuths of the other elements of the system: $\alpha_0 = 45°$, $\alpha_1 = 0°$, $\alpha_2 = 45°$, $\alpha_y = 0°$, $\alpha_{an} = 45°$. For quartz decoding plate the contrast $V_{S/-R}$ and the initial phase shift $\delta_S - \delta_R$ practically do not depend on the position z_d of the detector. For calcite plate, the contrast decreases when detector is shifted towards initial focusing point of the convergent beam (origin of the coordinate system). This effect is caused by increasing spatial separation of ordinary and extraordinary beams in the photodetector plane when it is shifted towards beam focus, see Fig. 5. For quartz decoding plate, the spatial separation between ordinary and extraordinary waves practically does not appear due to the much lower birefringence of this material (Fig. 5). The calculation results indicate that the detector should be placed possibly close to the decoding plate, however, the ability of the decoding plate to rotate should be preserved. In further analysis of the detection system it was assumed that the detector is in the middle between focusing point and the second surface of the birefringent plate ($z_d = 2.2$ cm).

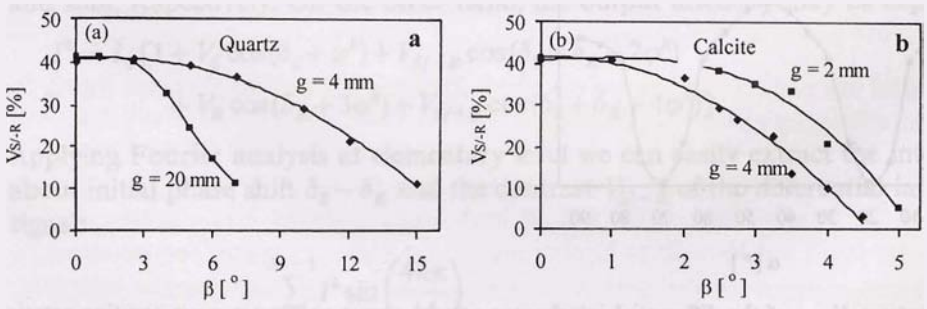

Fig. 11. Contrast $V_{S/-R}$ of the differential interference pattern versus aperture angle of the beam in the decoding system for quartz (a) and calcite (b) plates of different thickness. The calculations were carried out for the following system parameters: $\alpha_0 = 45°$, $\alpha_1 = 0°$, $\alpha_2 = 45°$, $\alpha_{bi} = 0°$, $\alpha_{an} = 45°$, $\theta = 0$.

We also analyzed how aperture angle β of a convergent beam influences the contrast $V_{S/-R}$ of the differential interference signal. In Figure 11 the contrast degradation is shown versus β for quartz and calcite plates of different thickness. The contrast decreases faster for calcite plates. For example, for 4 mm thick calcite plate the contrast drops to half of its initial value for $\beta = 3.2°$ while for quartz plate of the same thickness for $\beta = 12°$. The most important factor responsible for lowering the contrast versus β is a nonuniform distribution of the phase shift between ordinary and extraordinary waves in the photodetector plane, see Fig. 12.

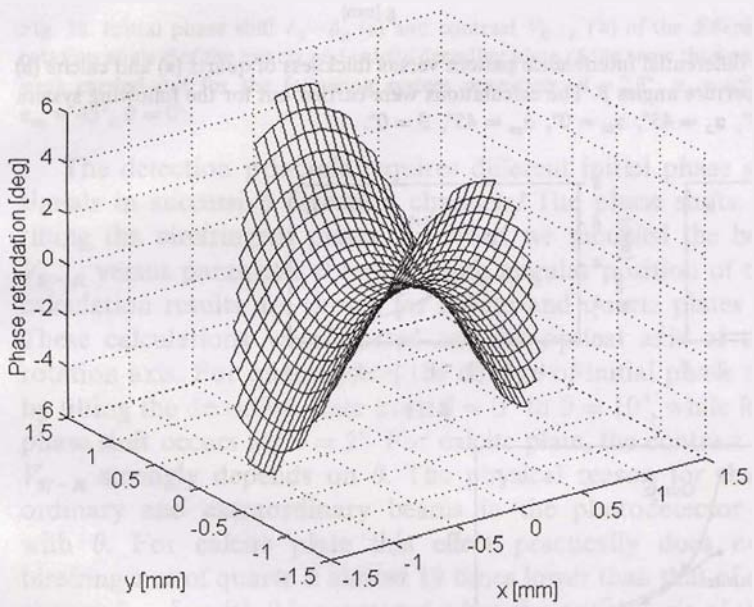

Fig. 12. Distribution of the phase shift $\delta_S - \delta_R$ for interfering ordinary and extraordinary wavefronts in the photodetector plane. The calculations were carried out for quartz decoding plate of thickness $g = 4$ mm. The other system parameters were as follows: $\beta = 2.5°$, $g = 4$ mm, $\alpha_0 = 45°$, $\alpha_1 = 0°$, $\alpha_2 = 45°$, $\alpha_{bl} = 0°$, $\alpha_{an} = 45°$, $\theta = 0°$.

The thickness of the compensating plate is the most important parameter of the decoding system. It determines the maximum retardation of the optical sensor that can be compensated in the decoding system and therefore, indirectly, the number of multiplexed sensors. Unfortunately, the increasing thickness of the decoding plate causes contrast degradation, Fig. 13. For every aperture angle β, we found the maximum thickness $g_{\max}$ of the decoding plate, for which contrast drops to 20%. In Fig. 14, we present $g_{\max}$ and also maximum retardation $R_{\max}$ that can be compensated by the plate of thickness $g_{\max}$ for quartz and calcite versus aperture angle β. The maximum retardation $R_{\max}$ was calculated according to the following expression:

$$R_{\max} = \frac{\Delta N g_{\max}}{\cdot} \tag{61}$$

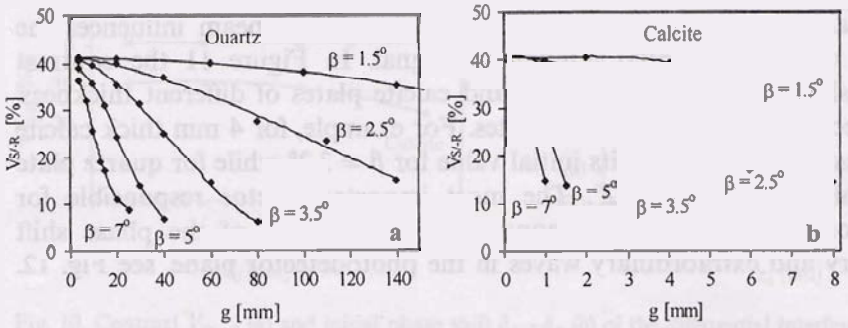

Fig. 13. Contrast $V_{S/-R}$ of the differential interference pattern versus thickness of quartz (a) and calcite (b) decoding plate for different aperture angles β. The calculations were carried out for the following system parameters: $\alpha_0 = 45°$, $\alpha_1 = 0°$, $\alpha_2 = 45°$, $\alpha_{bl} = 0°$, $\alpha_{an} = 45°$, $\theta = 0°$.

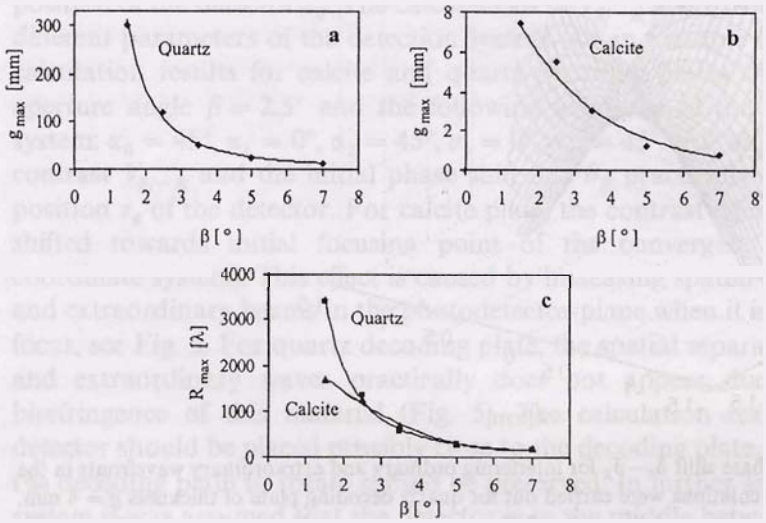

Fig. 14. Maximum thickness g_{max} of the quartz (a) and calcite (b) plate and maximum group retardation R_{max} that can be compensated using those plates versus aperture angle β (c). The calculations were carried out for the following system prameters: $\alpha_0 = 45°$, $\alpha_1 = 0°$, $\alpha_2 = 45°$, $\alpha_{bl} = 0°$, $\alpha_{an} = 45°$, $\theta = 0°$.

where $\Delta N = 0.00934$ and $\Delta N = 0.18789$ stand for the group birefringence, respectively for quartz and calcite at $\lambda_0 = 832.5$ nm [9]. The results presented in Fig. 14 show that for $\beta > 2.5°$ the R_{max} decreases with β in the same way for calcite and quartz plates. For lower aperture angles ($\beta < 2.5°$) higher contrast may be obtained for quartz compensating plates. In spite of contrast behaviour, one should note that to compensate retardations of the order of $10^3\ \lambda_0$ calcite rather than quartz plates should be applied. They are much thinner than quartz plates of the same retardation and therefore more practical to use. For lower retardations of the order of $10^2\ \lambda_0$ quartz plates are more practical to use because quartz is less expensive and much more resistant material than calcite.

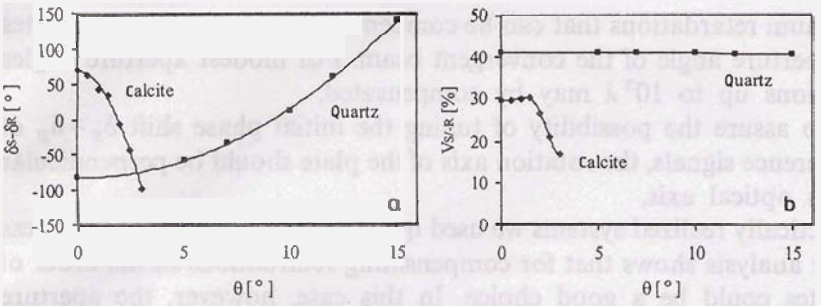

Fig. 15. Initial phase shift $\delta_S - \delta_R$ (a) and contrast $V_{S/-R}$ (b) of the different interference pattern versus rotation angle θ of the quartz and calcite decoding plate of the same thickness $g = 4$ mm. The calculations were carried out for the following system prameters: $\beta = 2.5°$, $\alpha_0 = 45°$, $\alpha_1 = 0°$, $\alpha_2 = 45°$, $\alpha_{bl} = 0°$, $\alpha_{an} = 45°$, $\theta = 0°$.

The detection principle requires different initial phase shifts of the interference signals in successive detection channels. The phase shifts $\delta_S - \delta_R$ are adjusted by tilting the birefringent plates, therefore, we modeled the behaviour of $\delta_S - \delta_R$ and $V_{S/-R}$ versus parameter θ representing angular position of the plate. In Fig. 15, the calculation results are shown for calcite and quartz plates of thickness $g = 4$ mm. These calculations were carried out for optical axis of the plate parallel to its rotation axis. For quartz plate, the change of initial phase shift by 100° is obtained by tilting the decoding plate from $\theta = 0°$ to $\theta = 10°$, while for calcite plate the same phase shift occurs for $\theta = 2°$. For calcite plate, the contrast of the differential signal $V_{S/-R}$ strongly depends on θ. The physical reason for that is the lateral shift of ordinary and extraordinary beams in the photodetector plane, which increases with θ. For calcite plate this effect practically does not appear because the birefringence of quartz is almost 19 times lower than that of calcite. The fastest phase change $\delta_S - \delta_R$ with θ is generated when the optical axis of the plate is perpendicular or parallel to its rotation axis. If these two axes are at $\pm 45°$ practically no phase shift is induced by tilting the plate. Therefore, it is important to control the orientation of the rotation axis with respect to the optical axis.

7. Summary

The results of modeling allowed us to draw the following conclusions concerning construction of the detection system assuring the highest contrast of the differential interference signal and therefore the highest operation range of the sensor:

1. The azimuths of successive birefringent elements of the fiber optic sensor and the detection system should alter by $\pm 45°$.

2. Directions $\vec{s}$ and $\vec{p}$ for the central ray incident on the beam splitter should overlap polarization directions of eigenmodes in the leading-out fiber or in the compensating plate.

3. The detectors should be placed possibly close to the decoding plate, however, the ability of decoding plates to rotate should be preserved.

4. The maximum retardations that can be compensated using birefringent plates decreases with aperture angle of the convergent beam. For modest aperture angles ($\beta \approx 2°$) retardations up to $10^3\,\lambda$ may by compensated.

5. In order to assure the possibility of tuning the initial phase shift $\delta_S - \delta_R$ of differential interference signals, the rotation axis of the plate should be perpendicular or parallel to its optical axis.

So far, in practically realized systems we used quartz decoding plates of thickness 4 to 20 mm. Our analysis shows that for compensating retardations of the order of $10^3\,\lambda$ calcite plates could be a good choice. In this case, however, the aperture angle β should not exceed 2°. Furthermore, due to stronger dependence of $\delta_S - \delta_R$ upon θ an accurate control of angular position of the calcite plate is required. As an acceptable error of initial phase $\delta_S - \delta_R$ adjustment is $\pm 5°$, the required resolution of angular position of the 5 mm thick ($10^3\,\lambda$) compensating calcite plate is 0.1°.

Acknowledgments – This work was supported by the Polish Committee for Scientific Research (KBN) under grant No. 8T10C 020 18.

References

[1] URBAŃCZYK W., NAWROCKA M.S., BOCK W.J., , Appl.Opt. (submitted for publication).
[2] BOCK W.J., NAWROCKA M.S., URBAŃCZYK W., *Coherence-multiplexed fiber-optic sensor systems for measurements of dynamic pressure and temperature changes*, to be published in Proc IEEE Instrumentation and Measurement Technology Conference in Budapest, Hungary, May 21–23, 2001.
[3] URBAŃCZYK W., BOCK W.J., Opt. Eng. **3** (1993), 2100..
[4] URBAŃCZYK W., KURZYNOWSKI P., WOŹNIAK A.W., BOCK W.J., Opt Commun. **135** (1997), 1.
[5] TROLINGER J.D., CHIPMAN R.A., WILSON D.K., Opt. Eng. **30** (1991), 461.
[6] GRATTAN K.T., V., MEGGIT B.T., *Optical Fiber Sensor Technology*, Chapman & Hall, London, Glasgow, Weinheim 1995, Chapt. 9, pp. 269–312.
[7] BORN M., WOLF E., *Principles of Optics*, 5th ed., Pergamon, Oxford, New York 1975, p. 316.
[8] YEH P., *Optical Waves in Layered Media*, John Wiley & Sons, New York, Chichester, Brisbane, 1988, Chapt. 9, pp. 201–253.
[9] GHOSH G., Opt. Commun. **163** (1999), 95.

Received January 20, 2001